NANO LETTERS

pubs.acs.org/NanoLett Letter

Manipulation of Rare-Earth-Ion Emission by Nonlinear-Mode Oscillation in a Lithium Niobate Microcavity

Jiangwei Wu, Yuxuan He, Qilin Yang, Xueyi Wang, Xiangmin Liu, Yong Geng, Guangcan Guo, Qiang Zhou,* Xianfeng Chen, and Yuping Chen*

Cite This: https://doi.org/10.1021/acs.nanolett.5c02562 Read Online

ACCESS | Metrics & More | Article Recommendations | Supporting Information

ABSTRACT: Optical microcavities provide opportunities to explore nonlinear effects and enable classic and quantum applications. This work investigates the manipulation of rare-earth-ion emission through nonlinear-mode oscillation in an erbium-doped thin-film lithium niobate microdisk cavity and demonstrates the changed laser performance. A pulsed transmission was generated with a detuned laser injected into the cavity. If the injected laser meets the pump band of the erbium ions, the output communication-band laser is also pulsed. The pulse's repetition rate and duration are changed with different detuned pump wavelengths and powers. All-optical temporal control of the emitter−cavity interaction paves the way to manipulation of quantum states with solid-state devices.

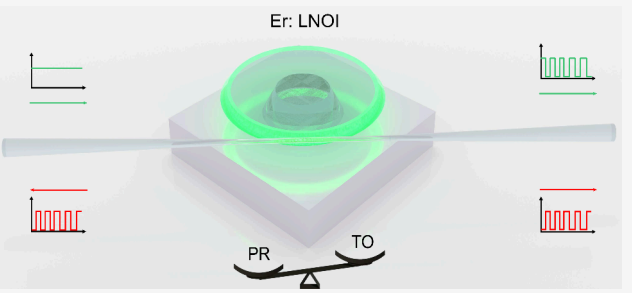

KEYWORDS: *rare-earth-ion emission, lithium niobate microcavity, nonlinear-mode oscillation, pulsed laser*

Research into rare-earth dopants has long been a pivotal focus in laser optoelectronics and quantum photonics.[1−5] Due to their distinctive electronic structures, long-lived excited states, and efficient emission in the near-infrared and visible spectral ranges, rare-earth ions (REIs) hold significant promise for applications in lasers, optical amplifiers, optical communications, and quantum storage. Their relevance is further underscored in the context of modern optical systems.[6−8] Precisely controlling the luminescent properties of these ions is crucial for optical signal modulation, optical signal processing, and applications in quantum communication and precision measurement.

The interaction between REIs and their surrounding environment plays a crucial role in determining their decay rates and emission characteristics. Researchers have made strides in introducing active and dynamic control over these environmental factors to effectively manipulate REI emissions.[9−16] For example, temperature changes can impact the width and intensity of the emission spectrum,[17] while electric fields can dynamically modify the energy levels of the ions, thereby influencing their emission behavior.[13] Although considerable progress has been made in these techniques, traditional methods often rely on complex external setups or intricate material treatments, which present challenges in terms of precision, scalability, and integration into miniaturized systems. Therefore, addressing these challenges to achieve more efficient and flexible emission control remains a paramount focus of ongoing research.

Lithium niobate (LN) is renowned for its strong electro-optical and nonlinear-optical effects, which provide versatile control mechanisms.[18−24] The rapidly advancing integration technology combined with REI doping makes thin-film lithium niobate (TFLN) an ideal medium for manipulating REI luminescence. Electrooptical modulation of the interaction between LN microcavities and doped ytterbium ions has been successfully demonstrated. This platform can help to shape the waveform of the emitter and encode quantum information.[14−16,25] Another phenomenon, called nonlinear-mode oscillation (NMO), which incorporates two nonlinear properties of LN,[26,27] has been investigated and may be useful for emission control. The NMO effect in TFLN arises from the competition between thermooptical (TO) nonlinearity and the photorefractive (PR) effect. The PR effect in LN is induced by a space-charge electric field, which originates from the drift and diffusion of carriers generated by the photoionization of trap states.[28] The recovery time of the PR effect varies from hours to several microseconds, depending on the LN crystal's thickness, orientation, and dopants.[29,30]

Here, we propose a method to manipulate REI emission using NMO in the microcavity. An erbium (Er)-doped TFLN

Received: May 12, 2025
Revised: June 9, 2025
Accepted: June 16, 2025

https://doi.org/10.1021/acs.nanolett.5c02562
Nano Lett. XXXX, XXX, XXX−XXX

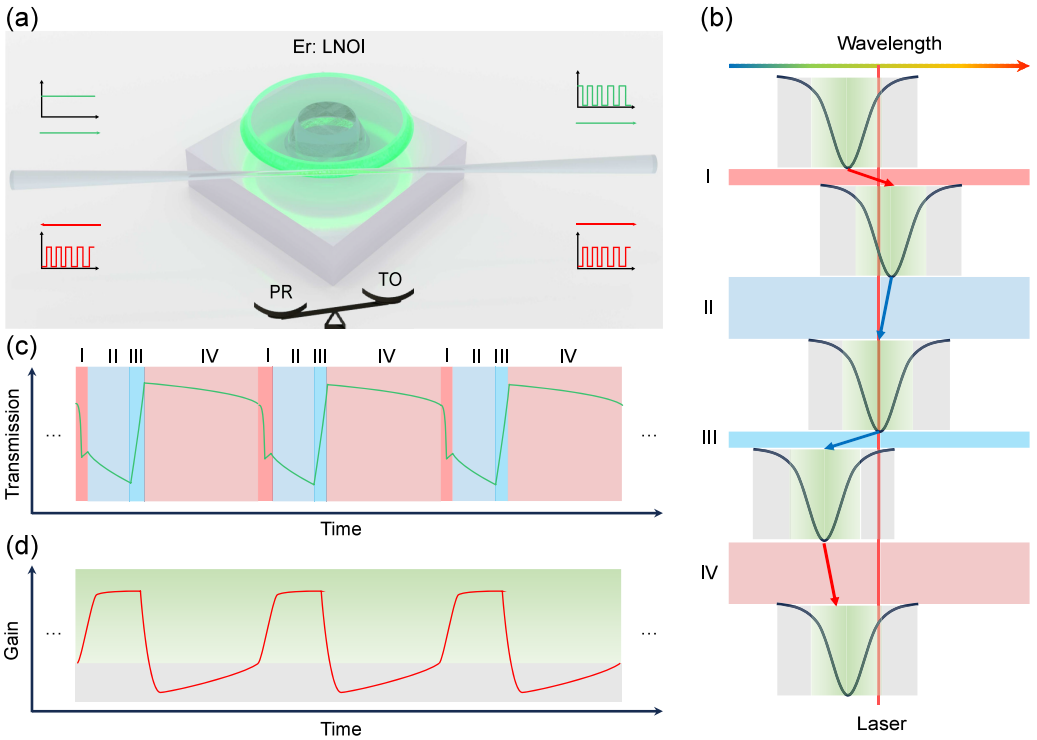

Figure 1. (a) Scheme of the periodic laser emission in an Er:TFLN microdisk through nonlinear oscillation. (b) Schematic of the time-dependent cavity resonance shift induced by the competition between the TO nonlinear and PR processes. (c) Time-dependent waveform of cavity transmission with the four stages denoted in part b. (d) Time-dependent gain for the generated laser in the cavity.

microdisk cavity is fabricated for the experiment. The NMO phenomenon can be observed when a finely tuned laser is injected. When the driven laser matches the pump band of the Er ions, a pulsed laser is generated with the pulsed pump, as shown in Figure 1a. The oscillation properties, such as the oscillating frequency (f) and mark−space ratio (MSR), are controllable by changing the detuned wavelength and power of the input laser. The duration and repetition rate of the generated laser are manipulated as a result. The pulse duration observed ranges from several seconds to hundreds of microseconds. Our results provide an all-optical way to temporally control the emission of REIs in a cavity. The method might find applications in quantum information processing and optical measurement.

The NMO in the TFLN microcavity could be divided into four stages, as shown in Figure 1b. A laser with red-detuned wavelength $\delta\omega_i$ couples into the cavity, where $\delta\omega_i = \omega_i - \omega_0$ is the wavelength detuning of input light frequency ω_i (i = p and l, which denote the laser in pump and the laser band of Er ions) to cavity resonance ω_0. The two nonlinear processes both start to respond. Because the TO effect has a faster response time (~10 μs) than the PR effect (several milliseconds), the cavity resonance would experience a fast red-shift $\delta\omega_T = g_T\eta_T|a(\delta\omega_0)|^2$ in stage I, where g_T is the photothermal coupling coefficient and η_T is the photothermal heating coefficient. The input laser is now at the blue detuned side of $\delta\omega_1 = \delta\omega_0 + \delta\omega_T$. In stage II, the space charge in the cavity accumulates and the induced electrooptical effect gradually pushes the resonance toward a shorter wavelength until the original cavity resonance $\delta\omega_2 = \delta\omega_1 - \delta\omega_E = 0$. The coupled optical energy reaches its maximum. The PR effect would continue to blue-shift the resonance, and the input laser power is reduced in stage III. The temperature in the cavity would decrease rapidly due to the fast relaxation rate of the TO effect. The heat-induced wavelength detuning $\delta\omega_T$ would vanish. The input laser has a larger detuned wavelength compared to the cavity resonance $\delta\omega_3 = \delta\omega_i - \delta\omega_E$. In stage IV, the accumulated space-charge field gradually relaxes because the minimum optical power is injected. The cavity resonance red-shifts to the same position as that in the first stage, and another oscillation starts. The detailed equations and corresponding simulation results are given in the Supporting Information (SI).

If the input laser is in the pump band of the Er ions and the pump power exceeds the threshold of NMO, the cavity resonance would shift periodically. The schematic transmission of the pump laser is shown in Figure 1c, in which the time scale of the fast response process is modified to show more detail. The pump power coupled into the cavity as well as the gain for the laser generation is time-dependent, as shown in Figure 1d. The oscillating gain coefficient has the same period as the pump transmission, while the shape is slightly different because the response for Er ions is governed by the rate equation. A detailed comparison is given in the SI. The green and gray blocks denote the regions where the gain coefficient exceeds the laser threshold or not. When the gain coefficient is in the green region, a laser in the communication band would be generated. As the coupled pump power decreases in stage III, the gain coefficient is decreased to the gray region and the laser is off. With this scheme, we obtained a pulsed laser. The above dynamics could be described using the coupled mode theory and rate equation, and a detailed description is given in the SI.

The NMO behaviors in both wavelength bands are investigated first. The experimental setup is shown in the SI. The results are shown in Figure 2. The loaded quality factors are 6.9×10^4 and 1.72×10^5, respectively (Figure 2a,e). Take

https://doi.org/10.1021/acs.nanolett.5c02562
Nano Lett. XXXX, XXX, XXX−XXX

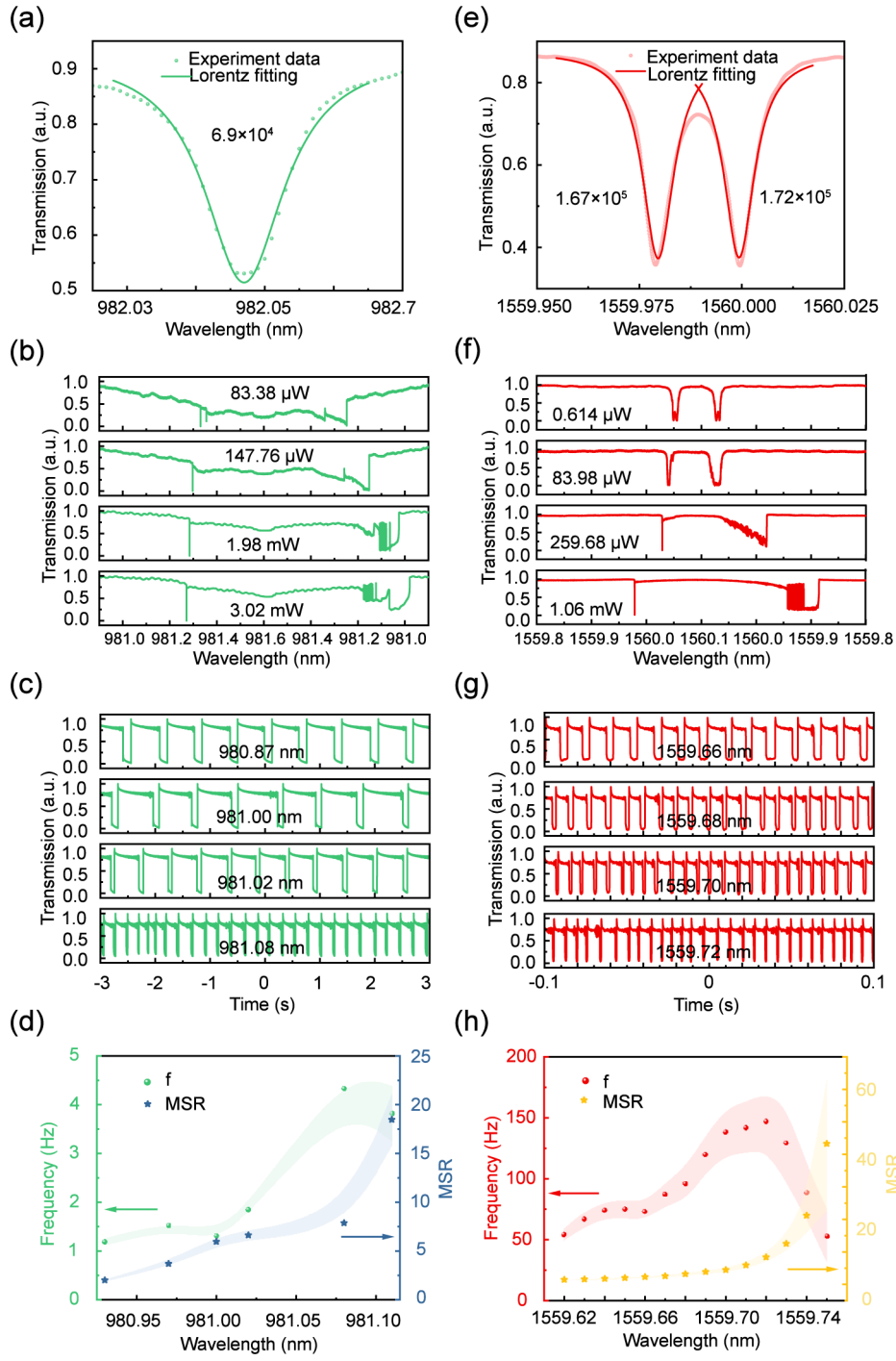

Figure 2. (a and e) Quality factor of the trigger mode at the pump and communication bands. (b and f) Laser-scanned cavity transmission spectrum at the pump and communication bands with increasing input optical power. (c and g) Time-dependent waveform of cavity transmission with constant input optical power and different laser wavelengths. (d and f) Nonlinear oscillation properties at different detuned wavelengths, where the colored bands represent the corresponding error bars.

the mode at ~982 nm as an example, which is in the pump band of the Er ions. We scan the input laser wavelength forward and then backward around the chosen mode at a certain speed. The transmission with different power is compared in Figure 2b. Because the scan range is fixed (980.8−981.6 nm, 0.1 nm/s), the blue shift of the optical mode is evident with the increasing input power, which is a sign of the PR effect. Also, the bistability-type behavior in the transmission is due to the TO effect. In the red-to-blue scanning range, the mode is broadened and starts to oscillate with a higher power. When the input laser is fixed in a certain detuned wavelength, the transmission would oscillate, as shown in Figure 2c. With different detuned wavelengths, the properties of the oscillation are different. Two parameters are chosen to characterize the behavior: f and MSR. The former describes how fast the oscillation is, and the latter shows more detail about the dynamics. As shown in Figure 1b,c. the mark region refers to stage IV, while the space region refers to

https://doi.org/10.1021/acs.nanolett.5c02562
Nano Lett. XXXX, XXX, XXX−XXX

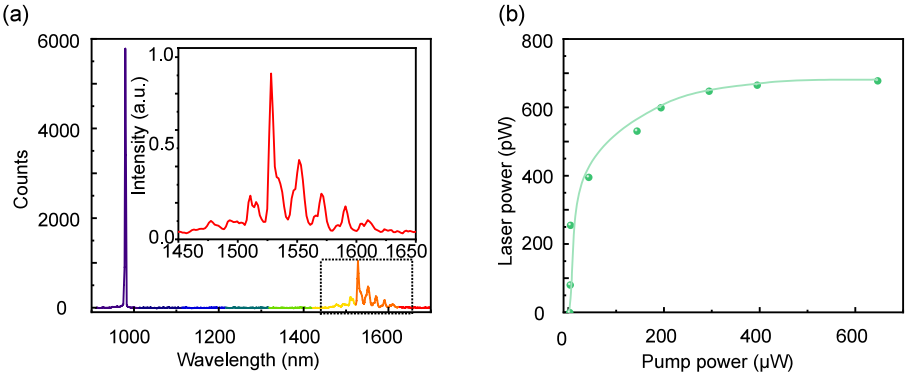

Figure 3. (a) Spectrum of the Er:TFLN microdisk under a tunable pump. The inset is the zoomed-in spectrum at the communication band. (b) Relationship between the laser power and tunable pump power.

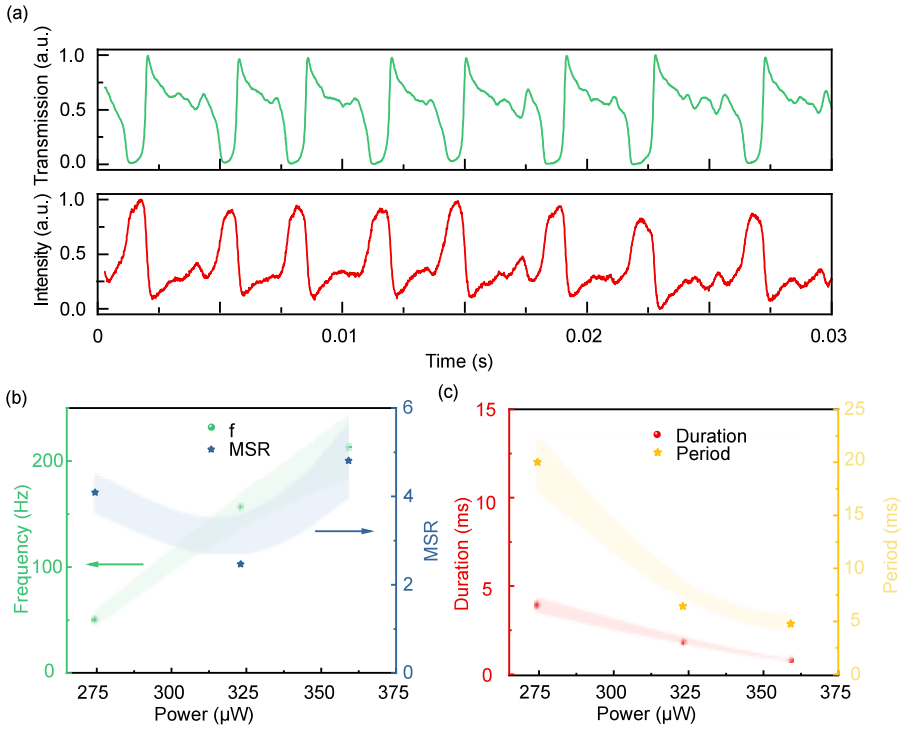

Figure 4. (a) Periodical laser emission with the pump wavelength at 973.58 nm. The pump signal is marked in green, and the laser is marked in red. Nonlinear oscillation properties (b) and the period and duration (c) of a pulsed laser with different pump power, where the colored bands represent the corresponding error bars.

regions I−III. The initial detuned wavelength and the coupled laser power would influence the MSR. Figure 2d shows the two parameters with fixed input powers and different detuned wavelengths. The MSR has an increasing trend with a longer wavelength, indicating a smaller ratio of the PR blue-shift time (stage II) in an oscillating period. The oscillating frequency first increases and then has a decreasing trend, which is mainly due to the relaxation time of the PR effect (stage IV). We also analyze the competing behavior in the communication band, as shown in Figure 2e−h. The results reveal a similar pattern. With a larger loaded quality factor (1.72×10^5), the threshold for oscillation is lowered.

The laser properties of the Er-doped microdisk are examined, and the result is shown in Figure 3. We tune the pump wavelength to a cavity mode and fix it. The output spectrum covering the pump and laser bands is shown in Figure 3a. The inset is the zoomed-in spectrum around the communication band. Several lasing peaks are matched with the free spectral range of the cavity. Although the cavity supports multimode lasing, we chose the maximum laser peak to achieve the pump−laser relationship (Figure 3b). The lasing threshold is around 3.5 μW. The saturation effect is obvious when the pump power exceeds 200 μW. It is worth noting that the threshold for the NMO (over 1 mW) is always larger than the saturation pump power, paving the way to achieve a pulsing laser.

When the input laser is in the pump band of the Er ions, the laser power exceeds the threshold for NMO. We could obtain a pulsed laser, as shown in Figure 4a. The difference in the oscillation frequency and MSR between the two results is due to the different input pump power and detuned wavelength. The pulse duration of the generated laser in Figure 4a is around 800 μs. We change the input pump power with fixed wavelength detuning (concerning the resonance at each input

https://doi.org/10.1021/acs.nanolett.5c02562
Nano Lett. XXXX, XXX, XXX−XXX

power) and obtain the frequency−pump power and MSR−pump power relationships, as shown in Figure 4b. Simultaneously, the period and duration of the pulsed laser are achieved and are shown in Figure 4c. The dependence of the NMO on the input power and detuned wavelength enables convenient manipulation of REI emission.

In conclusion, we designed an all-optical method to manipulate REI emission. The intrinsic properties of REI-doped TFLN are investigated to realize a compact, convenient, and highly tunable manipulator. The rare-earth emitters are coupled with the microcavity, and the NMO temporally controls the cavity resonance. This maneuvering capability paves the way for integrated quantum technology. Potential applications include controllable quantum interfaces between solid-state spins, single telecom photons, and quantum gates between REI qubits coupled to an optical cavity.

■ ASSOCIATED CONTENT

Supporting Information

The Supporting Information is available free of charge at https://pubs.acs.org/doi/10.1021/acs.nanolett.5c02562.

Dynamic equations for NMO, experiment setup, detailed dynamics due to REIs, PR effect concerning two wavelengths, and lifetime of the REIs (PDF)

■ AUTHOR INFORMATION

Corresponding Authors

Qiang Zhou − *Institute of Fundamental and Frontier Sciences, University of Electronic Science and Technology of China, Chengdu 610054, China; CAS Key Laboratory of Quantum Information, University of Science and Technology of China, Hefei 230026, China; School of Optoelectronic Science and Engineering, University of Electronic Science and Technology of China, Chengdu 610054, China*; Email: zhouqiang@uestc.edu.cn

Yuping Chen − *School of Physics and Astronomy, State Key Laboratory of Photonics and Communications, Shanghai Jiao Tong University, Shanghai 200240, China*; orcid.org/0000-0003-3969-7119; Phone: +86-13816373910; Email: ypchen@sjtu.edu.cn

Authors

Jiangwei Wu − *School of Physics and Astronomy, State Key Laboratory of Photonics and Communications, Shanghai Jiao Tong University, Shanghai 200240, China*

Yuxuan He − *School of Physics and Astronomy, State Key Laboratory of Photonics and Communications, Shanghai Jiao Tong University, Shanghai 200240, China*

Qilin Yang − *Institute of Fundamental and Frontier Sciences, University of Electronic Science and Technology of China, Chengdu 610054, China*

Xueyi Wang − *School of Physics and Astronomy, State Key Laboratory of Photonics and Communications, Shanghai Jiao Tong University, Shanghai 200240, China*

Xiangmin Liu − *School of Physics and Astronomy, State Key Laboratory of Photonics and Communications, Shanghai Jiao Tong University, Shanghai 200240, China*

Yong Geng − *Institute of Fundamental and Frontier Sciences, University of Electronic Science and Technology of China, Chengdu 610054, China*

Guangcan Guo − *Institute of Fundamental and Frontier Sciences, University of Electronic Science and Technology of China, Chengdu 610054, China; CAS Key Laboratory of Quantum Information, University of Science and Technology of China, Hefei 230026, China*

Xianfeng Chen − *School of Physics and Astronomy, State Key Laboratory of Photonics and Communications, Shanghai Jiao Tong University, Shanghai 200240, China; Collaborative Innovation Center of Light Manipulations and Applications, Shandong Normal University, Jinan 250358, China*; orcid.org/0000-0002-1301-7448

Complete contact information is available at: https://pubs.acs.org/10.1021/acs.nanolett.5c02562

Author Contributions

J.W., Y.H., Q.Y., and X.W. contributed equally to this work. Y.C. conceived the project. J.W. and Q.Y. carried out numerical simulation. J.W. fabricated the sample. J.W., X.W., and Y.H. carried out the optical characterization. J.W. and Y.H. analyzed the data. J.W., Y.H., and Q.Y. wrote the manuscript with comments from X.L., Y.G., G.G., Q.Z., X.C., and Y.C. Y.C. supervised the project. All authors contributed to the discussion of experimental results.

Notes

The authors declare no competing financial interest.

■ ACKNOWLEDGMENTS

This work was supported by the National Natural Science Foundation of China (12134009, 12474335, and 12192252). Sichuan Science and Technology Program (Nos. 2023YFSY0058, 2023YFSY0061, and 2024YFHZ0369), and National Natural Science Foundation of China (No. 62475039). The authors thank Prof. Jintian Lin from East China Normal University for his technical support and the Center for Advanced Electronic Materials and Devices of Shanghai Jiao Tong University for its support in device fabrication.

■ REFERENCES

(1) Bao, R.; Fang, Z.; Liu, J.; Liu, Z.; Chen, J.; Wang, M.; Wu, R.; Zhang, H.; Cheng, Y. An Erbium-Doped Waveguide Amplifier on Thin Film Lithium Niobate with an Output Power Exceeding 100 mW. *Laser Photonics Rev.* **2025**, *19*, 2400765.

(2) Liu, Y.; Qiu, Z.; Ji, X.; Bancora, A.; Lihachev, G.; Riemensberger, J.; Wang, R. N.; Voloshin, A.; Kippenberg, T. J. A fully hybrid integrated erbium-based laser. *Nat. Photonics* **2024**, *18*, 829−835.

(3) Saglamyurek, E.; Sinclair, N.; Jin, J.; Slater, J. A.; Oblak, D.; Bussieres, F.; George, M.; Ricken, R.; Sohler, W.; Tittel, W. Broadband waveguide quantum memory for entangled photons. *Nature* **2011**, *469*, 512−515.

(4) Zhang, X.; Zhang, B.; Wei, S.; Li, H.; Liao, J.; Li, C.; Deng, G.; Wang, Y.; Song, H.; You, L.; Jing, B.; Chen, F.; Guo, G.; Zhou, Q. Telecom-band−integrated multimode photonic quantum memory. *Sci, Adv.* **2023**, *9*, eadf4587.

(5) Zhong, T.; Kindem, J. M.; Bartholomew, J. G.; Rochman, J.; Craiciu, I.; Miyazono, E.; Bettinelli, M.; Cavalli, E.; Verma, V.; Nam, S. W.; et al. Nanophotonic rare-earth quantum memory with optically controlled retrieval. *Science* **2017**, *357*, 1392−1395.

(6) Jia, Y.; Wu, J.; Sun, X.; Yan, X.; Xie, R.; Wang, L.; Chen, Y.; Chen, F. Integrated photonics based on rare-earth ion-doped thin-film lithium niobate. *Laser Photonics Rev.* **2022**, *16*, 2200059.

(7) Thiel, C. W.; Böttger, T.; Cone, R. Rare-earth-doped materials for applications in quantum information storage and signal processing. *Journal of luminescence* **2011**, *131*, 353−361.

(8) Zhong, T.; Goldner, P. Emerging rare-earth doped material platforms for quantum nanophotonics. *Nanophotonics* **2019**, *8*, 2003−2015.

(9) Jin, C.-Y.; Johne, R.; Swinkels, M. Y.; Hoang, T. B.; Midolo, L.; Van Veldhoven, P. J.; Fiore, A. Ultrafast non-local control of spontaneous emission. *Nat. Nanotechnol.* **2014**, *9*, 886−890.
(10) Reserbat-Plantey, A.; Schädler, K. G.; Gaudreau, L.; Navickaite, G.; Güttinger, J.; Chang, D.; Toninelli, C.; Bachtold, A.; Koppens, F. H. Electromechanical control of nitrogen-vacancy defect emission using graphene NEMS. *Nat. Commun.* **2016**, *7*, 10218.
(11) Tian, F.; Sumikura, H.; Kuramochi, E.; Taniyama, H.; Takiguchi, M.; Notomi, M. Optomechanical oscillator pumped and probed by optically two isolated photonic crystal cavity systems. *Opt. Express* **2016**, *24*, 28039−28055.
(12) Cotrufo, M.; Midolo, L.; Zobenica, Ž.; Petruzzella, M.; Van Otten, F. W.; Fiore, A. Nanomechanical control of optical field and quality factor in photonic crystal structures. *Phys. Rev. B* **2018**, *97*, 115304.
(13) Cano, D.; Ferrier, A.; Soundarapandian, K.; Reserbat-Plantey, A.; Scarafagio, M.; Tallaire, A.; Seyeux, A.; Marcus, P.; Riedmatten, H. d.; Goldner, P.; Koppens, F. H. L.; Tielrooij, K.-J. Fast electrical modulation of strong near-field interactions between erbium emitters and graphene. *Nat. Commun.* **2020**, *11*, 4094.
(14) Xia, K.; Sardi, F.; Sauerzapf, C.; Kornher, T.; Becker, H.-W.; Kis, Z.; Kovacs, L.; Dertli, D.; Foglszinger, J.; Kolesov, R.; et al. Tunable microcavities coupled to rare-earth quantum emitters. *Optica* **2022**, *9*, 445−450.
(15) Yang, L.; Wang, S.; Shen, M.; Xie, J.; Tang, H. X. Controlling single rare earth ion emission in an electro-optical nanocavity. *Nat. Commun.* **2023**, *14*, 1718.
(16) Wang, Y.; Xie, Q.; Jiang, C. Modulation of the emission spectrum of rare-earth ions using inverse-designed photonic crystals cavities. *Opt. Express* **2024**, *32*, 4346−4364.
(17) Wu, J.; Yan, X.; Wang, X.; Yuan, T.; Chen, C.; Li, H.; Chen, Y.; Chen, X. Efficient integrated amplifier-assisted laser on erbium-doped lithium niobate. *ACS Photonics* **2024**, *11*, 2114−2122.
(18) Luo, R.; He, Y.; Liang, H.; Li, M.; Lin, Q. Highly tunable efficient second-harmonic generation in a lithium niobate nanophotonic waveguide. *Optica* **2018**, *5*, 1006−1011.
(19) Wang, C.; Zhang, M.; Chen, X.; Bertrand, M.; Shams-Ansari, A.; Chandrasekhar, S.; Winzer, P.; Lončar, M. Integrated lithium niobate electro-optic modulators operating at CMOS-compatible voltages. *Nature* **2018**, *562*, 101−104.
(20) Lin, J.; Yao, N.; Hao, Z.; Zhang, J.; Mao, W.; Wang, M.; Chu, W.; Wu, R.; Fang, Z.; Qiao, L.; et al. Broadband quasi-phase-matched harmonic generation in an on-chip monocrystalline lithium niobate microdisk resonator. *Physical review letters* **2019**, *122*, 173903.
(21) Wang, C.; Zhang, M.; Yu, M.; Zhu, R.; Hu, H.; Loncar, M. Monolithic lithium niobate photonic circuits for Kerr frequency comb generation and modulation. *Nat. Commun.* **2019**, *10*, 978.
(22) Li, M.; Ling, J.; He, Y.; Javid, U. A.; Xue, S.; Lin, Q. Lithium niobate photonic-crystal electro-optic modulator. *Nat. Commun.* **2020**, *11*, 4123.
(23) Wang, X.; Yuan, T.; Wu, J.; Chen, Y.; Chen, X. Enhanced Temperature Sensing by Multi-Mode Coupling in an On-Chip Microcavity System. *Laser Photonics Rev.* **2024**, *18*, 2300760.
(24) Liu, X.; Chen, C.; Ge, R.; Wu, J.; Chen, X.; Chen, Y. Ultralow-Threshold Lithium Niobate Photonic Crystal Nanocavity Laser. *Nano Lett.* **2025**, *25*, 6454−6460.
(25) Ródenas, A.; Zhou, G.; Jaque, D.; Gu, M. Rare-Earth Spontaneous Emission Control in Three-Dimensional Lithium Niobate Photonic Crystals. *Adv. Mater.* **2009**, *21*, 3526−3530.
(26) Sun, X.; Liang, H.; Luo, R.; Jiang, W. C.; Zhang, X.; Lin, Q. Nonlinear optical oscillation dynamics in high-Q lithium niobate microresonators. *Opt. Express* **2017**, *25*, 13504−13516.
(27) Wang, X.; Wu, J.; Chen, C.; Yuan, T.; Chen, Y.; Chen, X. Enhanced sensing resolution with microcavity mode oscillation generated by thermal-optic and photorefractive nonlinearity. *Appl. Phys. Lett.* **2024**, *124*, 061108.
(28) Medrano, C.; Günter, P. *CRC Handbook of Laser Science and Technology*; CRC Press, 2020; Supplement 2, pp 431−463.
(29) Ren, X.; Lee, C.-H.; Xue, K.; Ou, S.; Yu, Y.; Chen, Z.; Yu, M. Photorefractive and pyroelectric photonic memory and long-term stability in thin-film lithium niobate microresonators. *npj Nanophotonics* **2025**, *2*, 1.
(30) Kong, Y.; Liu, S.; Xu, J. Recent advances in the photorefraction of doped lithium niobate crystals. *Materials* **2012**, *5*, 1954−1971.

https://doi.org/10.1021/acs.nanolett.5c02562
Nano Lett. XXXX, XXX, XXX−XXX